Beam-Driven Ion-Cyclotron Modes in the Scrape-off Layer of a Field-Reversed Configuration

B. S. Nicks,[1, a)] A. Necas,[2, b)] and T. Tajima[1, 2, c)]
[1)] *Department of Physics and Astronomy, University of California, Irvine, California 92617, USA*
[2)] *TAE Technologies, Inc., Foothill Ranch, California 92610, USA*

(Dated: 29 May 2020)

In the scrape-off-layer (SOL) of a field-reversed configuration (FRC), neutral beam injection can drive modes in the vicinity of the ion-cyclotron frequency. Depending on their properties, these modes can have differing macroscopic effects on the plasma. This work examines the linear properties of the various categories of ion-cyclotron modes that can be excited in the SOL environment, taking an ion beta of 10%. Propagation angle and beam injection angle are scanned from 0° to 90° with respect to the external magnetic field. The nonlinear physics of these modes, particularly ion acceleration with consequences for plasma stability and fusion reactivity, as are also examined. Primarily the work considers a deuterium plasma and hydrogen beam, but the case of a boron-11 plasma and hydrogen beam is also briefly considered.

I. INTRODUCTION

In a field-reversed magnetic configuration (FRC), a compact toroid of (reversed) closed field lines is embedded in a magnetic mirror[1]. In addition to providing a relative technological simplicity, this arrangement produces several distinct beneficial plasma properties, such high plasma beta and large particle orbits. One strategy of augmenting this base conception of an FRC is the injection of neutral beams nearly perpendicularly to the axial magnetic field, as in the C-2U machine[2]. In this case, the beam ion pressure is equal to or greater than the thermal plasma pressure, and the fast beam ions possess machine-sized orbits. This intense fast-ion pressure forms an internal spine that stabilizes the FRC against macro-instabilities. Such a scheme was the vision of Norman Rostoker[3].

While the beam stabilizes harmful macro-scale modes, it can also drive microscopic modes, warranting an examination of beam-plasma interaction with regard to micro-instabilities. An interesting class of these modes which may be preferred are those with frequencies in the vicinity of the ion-cyclotron (IC) frequency or its harmonics. In the high-beta FRC core, the preferred of such modes is the Alfvén-ion cyclotron (AIC) mode[4], but in the lower-beta scrape-off-layer (SOL), electrostatic modes such as ion-Bernstein modes[5,6] or other IC modes[7] may be excited. The SOL is a thick region of open field lines outside the FRC core that nonetheless contains considerable plasma and beam pressure. Three chief factors establish the SOL as the more pressing to examine in this work. First, the closed field lines in the core mean that wave-induced disruptions of these kinds are essentially benign. Second, the beam-plasma interaction is likely strongest in the SOL due to the distribution of beam orbits. Third, and perhaps more importantly, the electrostatic modes that can be driven in the SOL can potentially generate a large tail of fast background ions, which has important bearing for fusion enhancement[8], as is elaborated below. A more in-depth analysis of the nonlinear physics of this ion acceleration can be found elsewhere[9]. For this work, we thus confine our attention to the SOL, and our goal is to examine the various IC modes that can exist in this environment.

Ion-cyclotron waves can be broadly divided into two categories: electrostatic and electromagnetic. While the former tend to propagate perpendicularly to the magnetic field, the latter are more strongly associated with propagation parallel to the magnetic field. A large quantity of work on electrostatic IC modes has focused on instabilities from a fast beam population, both in the case of particles streaming along the magnetic field[5,6,10–13] and particles with a substantial perpendicular component[14–16]. In particular, the emission of IC waves driven by fast fusion ions via the magnetoacoustic instability has been studied extensively[17–20]. In this same context, IC heating has been pursued as a means of heating beam ions[21]. Observations of accelerated ion populations in the magnetosphere and ionosphere[22–24] has also motivated study of electrostatic modes. Electromagnetic IC modes have similarly been studied in the contexts of space[25–29] and fusion[4,30,31] physics. In this study, we marshal this large body of knowledge to build an understanding of the beam-driven IC physics possible in the SOL environment of an FRC. To our knowledge, this has not been coherently done before.

To this end, we employ 1D particle-in-cell simulations to scan the full angular span of beam injection and mode propagation, dividing this scan into qualitative regimes for comprehension of the linear physics[32,33]. For each regime, the nonlinear acceleration of background ions is also briefly examined. In particular, a distinction is made between modes that increase the bulk ion temperature and those that merely generate a tail of fast ions, the for-

[a)] Electronic mail: bnicks@uci.edu
[b)] Electronic mail: anecas@tae.com
[c)] Electronic mail: ttajima@uci.edu

mer being generally conducive to anomalous transport, macro-instabilities, and turbulence, and the latter being relatively benign.

This difference derives from the typical phase velocities of the waves excited. In cases where the wave phase velocity lies within the ion thermal distribution, the wave couples to the bulk motion of the ions, potentially causing disruptions of the plasma. The saturation of the wave follows familiar quasilinear theory[34,35]. In contrast, if the phase velocity is much larger than the ion thermal speed, the saturation mechanism becomes that of wakefield physics[36], and the wave trapping velocity[37] approaches the wave phase velocity. The wave then exists in a robust state and accelerates a tail of ions to very high energy without inciting plasma disruptions. Such modes can be highly beneficial for a fusion plasma, dramatically increasing the fusion rate while preserving confinement[8]. The possible of seeding such modes through density bunching of the beam is also explored by considering a beam population initialized with density modulations to resonantly excite the desired mode.

The organization of the paper is as follows. Section II presents the broad kinetic analytical theory of beam-driven waves in plasmas. Section III establishes the details of the simulation scheme and plasma parameters used in this work. Section IV then explores the regime of IC waves propagating parallel to the magnetic field, and section V treats oblique propagation. Section VI then completes the angular parameter scan by examining perpendicular propagation and the interesting nonlinear physics that results. Section VII considers the effectiveness of seeding a desired mode to increase the efficiency of its excitation and acceleration of background ions. Section VIII then briefly extends the preceding results to that with a proton-boron-11 plasma. Finally, section IX makes concluding remarks.

II. ANALYTICAL MODELING OF IC MODES

The foundation of this work is the modeling of kinetic ion-cyclotron waves in an experimentally relevant geometry and parameter regime. To this end, we make use of the essentially 1D geometry of the SOL of the C-2U FRC and consider a homogeneous plasma in a uniform magnetic field. This situation can be described in analytical theory, from which the major properties can be extracted. The kinetic beam effects are of particular concern, and so in general it will be necessary to treat an arbitrary beam injection and wave propagation angle. Additionally, to obtain a relatively realistic picture of the robustness of excitations in various regimes of these angular parameters, the beam is given a thermal spread in addition to its drift component. Including this complication produces substantially more experimentally relevant mode structure. This concern requires a substantial analytical effort and is a somewhat novel feature of this study. We thus set now to tackling the analytical formalism underlying this work.

The analytical theory of linear plasma waves begins with the relation $\vec{D} = \boldsymbol{\epsilon} \cdot \vec{E}$[32,33], where $\vec{D}$ is the displacement electric field in a medium (plasma), and $\boldsymbol{\epsilon}$ is the dielectric tensor. (It is assumed that the medium has a linear response to the electric field $\vec{E}$ in the limit of low-amplitude waves.) Arrow accents denote vectors, and bold font denotes matrices. By expressing Maxwell's equations in terms of complex Fourier amplitudes, it can be shown that $\boldsymbol{\epsilon}$ determines the allowable waves in a plasma. For a wave with wavevector $\vec{k}$ and frequency ω, the general plasma dispersion relation is given by

$$\det |\boldsymbol{\Delta}(\vec{k}, \omega)| = 0, \tag{1}$$

where

$$\boldsymbol{\Delta}(\vec{k}, \omega) = \boldsymbol{\epsilon}(\vec{k}, \omega) - \left(\frac{\omega/k}{c}\right)^2 \left(\boldsymbol{I} - \frac{\vec{k}\vec{k}}{k^2}\right). \tag{2}$$

The electric field polarization is given by solving for the eigenvectors of $\boldsymbol{\Delta} \cdot \vec{E} = 0$ once $\vec{k}$ and ω are determined by Eq. 1. The magnetic field polarization is then given by $\vec{B} = (c/\omega)(\vec{k} \times \vec{E})$.

The dielectric tensor $\boldsymbol{\epsilon}$ is thus chief object of interest for determining the allowed $\vec{k}$ and ω. While a simpler, scalar function containing only information about electrostatic (longitudinal) waves can be found by $\epsilon(\vec{k}, \omega) = [\vec{k} \cdot \boldsymbol{\epsilon}(\vec{k}, \omega) \cdot \vec{k}]/k^2$, the relatively high ion beta considered here ($\beta = 0.1$) necessitates the inclusion of the full tensor, which contains the full wave information, including both electrostatic and electromagnetic waves or hybridized combinations thereof. The full tensor can be conveniently divided among the contributions from each plasma species σ according to

$$\boldsymbol{\epsilon}(\vec{k}, \omega) = \boldsymbol{I} - \sum_{\sigma} \boldsymbol{\epsilon}_{\sigma}, \tag{3}$$

where

$$\boldsymbol{\epsilon}_{\sigma}(\vec{k}, \omega) = \left(\frac{\omega_{\sigma}}{\omega}\right)^2 \left[\boldsymbol{I} + \sum_{n=-\infty}^{\infty} \int \left(\frac{n\Omega_{\sigma}}{v_{\perp}} \frac{\partial f_{\sigma}}{\partial v_{\perp}} + k_{\parallel} \frac{\partial f_{\sigma}}{\partial v_{\parallel}}\right) \times \frac{\boldsymbol{\Pi}_{\sigma}(v_{\perp}, v_{\parallel}; n)}{n\Omega_{\sigma} + k_{\parallel} v_{\parallel} - \omega - i\eta} d^3 v\right] \tag{4}$$

for a homogeneous plasma in a uniform magnetic field $\vec{B}_0 \parallel \hat{z}$ with wavevector $\vec{k} = k_{\perp}\hat{x} + k_{\parallel}\hat{z}$. The angle $0^{\circ} \leq \theta_k \leq 90^{\circ}$ denotes the direction of $\vec{k}$ with respect to $\vec{B}_0$, with which $k_{\perp} = k \sin\theta_k$ and $k_{\parallel} = k \cos\theta_k$. Note that this coordinate frame is different from that used in the simulation scheme, as is described section III. The characteristic frequencies for each species are the species plasma frequency $\omega_{\sigma} = \sqrt{4\pi n_{\sigma} q_{\sigma}^2 / m_{\sigma}}$ and cyclotron frequency $\Omega_{\sigma} = q_{\sigma} B_0 / m_{\sigma} c$, where q_{σ}, m_{σ}, and

n_σ are respectively the charge, mass, and number density of a species. The total plasma frequency is given by $\omega_p^2 = \sum_\sigma \omega_\sigma^2 \approx \omega_e^2$. The tensor $\mathbf{\Pi}_\sigma$ is given by

$$\mathbf{\Pi}_\sigma = \begin{bmatrix} \left(\frac{n\Omega_\sigma}{k_\perp}\right)^2 J_n^2 & iv_\perp \frac{n\Omega_\sigma}{k_\perp} J_n J_n' & v_\parallel \frac{n\Omega_\sigma}{k_\perp} J_n^2 \\ -iv_\perp \frac{n\Omega_\sigma}{k_\perp} J_n J_n' & v_\perp^2 (J_n')^2 & -iv_\parallel v_\perp J_n J_n' \\ v_\parallel \frac{n\Omega_\sigma}{k_\perp} J_n^2 & iv_\parallel v_\perp J_n J_n' & v_\parallel^2 J_n^2 \end{bmatrix}, \tag{5}$$

where $J_n \equiv J_n(\mathsf{z})$, $\mathsf{z} \equiv k_\perp v_\perp/\Omega_\sigma$, and $J_n' \equiv dJ_n(\mathsf{z})/d\mathsf{z}$. The quantity η represents a small, adiabatic turning-on of a field perturbation. The integral is done over all velocity space, with in general $d^3v = 2\pi v_\perp \, dv_\perp \, dv_\parallel$.

The species velocity distribution function is given denoted by f_σ, and we must now provide a notation to differentiate species. Let the subscripts i, e, and b respectively indicate background ions, electrons, and beam ions. References henceforth to simply "ions" refer to the background ions. The ions and electrons are given Maxwellian distributions with isotropic temperature. For $\sigma \in \{i, e\}$,

$$f_\sigma(v_\perp, v_\parallel) = \frac{v_\perp}{(2\pi)^{3/2} v_{t\sigma}^3} \exp\left(-\frac{v_\perp^2 + v_\parallel^2}{2v_{t\sigma}^2}\right), \tag{6}$$

where $v_{t\sigma} = \sqrt{T_\sigma/m_\sigma}$ is the characteristic thermal speed for a species σ with temperature T_σ. This distribution obeys the normalization $\int f_\sigma(v_\perp, v_\parallel)\, d^3v = 1$. Substituting the ion and electron expressions for f_σ into Eq. 4 and carrying out the integration over velocity space yields (for $\sigma \in \{i, e\}$)

$$\epsilon_\sigma(\vec{k}, \omega) = -\left(\frac{\omega_\sigma}{\omega}\right)^2 \left[z_{\sigma 0}^2 \hat{z}\hat{z} + \sum_{n=-\infty}^{\infty} z_{\sigma 0} \mathcal{Z}(z_{\sigma n}) \boldsymbol{\pi}(\beta_\sigma, z_{\sigma n}; n) \right], \tag{7}$$

where

$$z_{\sigma n} \equiv \frac{\omega - n\Omega_\sigma}{|k_\parallel| v_{t\sigma}}, \tag{8}$$

and $\beta_\sigma \equiv (k_\perp v_{t\sigma}/\Omega_\sigma)^2 = (k_\perp \rho_\sigma)^2$ (where for $\sigma \in \{i, e\}$, the Larmor radius is defined as $\rho_\sigma = v_{t\sigma}/\Omega_\sigma$). The modified tensor $\boldsymbol{\pi}$ can be expressed as

$$\boldsymbol{\pi}(\beta_\sigma, z_{\sigma n}; n) = \begin{bmatrix} \pi_{11} & \pi_{12} & \pi_{13} \\ -\pi_{21} & \pi_{22} & \pi_{23} \\ \pi_{13} & -\pi_{23} & \pi_{33} \end{bmatrix}, \tag{9}$$

where the distinct elements are

$$\pi_{11} = \frac{n^2}{\beta_\sigma} \Lambda_n(\beta_\sigma), \tag{10a}$$

$$\pi_{12} = \pi_{12} = in\Lambda_n'(\beta_\sigma), \tag{10b}$$

$$\pi_{13} = n \frac{z_{\sigma n}}{\beta_\sigma^{1/2}} \Lambda_n(\beta_\sigma), \tag{10c}$$

$$\pi_{22} = \frac{n^2}{\beta_\sigma} \Lambda_n(\beta_\sigma) - 2\beta_\sigma \Lambda_n'(\beta_\sigma) \tag{10d}$$

$$\pi_{23} = -iz_{\sigma n} \beta_\sigma^{1/2} \Lambda_n'(\beta_\sigma) \tag{10e}$$

and

$$\pi_{33} = z_{\sigma n}^2 \Lambda_n(\beta_\sigma), \tag{10f}$$

where $\Lambda_n(x) = I_n(x)e^{-x}$ and $I_n(x)$ is the modified Bessel function of index n. The function $\mathcal{Z}(z)$ is a modified version of the plasma dispersion function[38] and is defined as

$$\mathcal{Z}(z) = \frac{1}{(2\pi)^{1/2}} \int_{-\infty}^{\infty} \frac{e^{-\zeta^2/2}}{\zeta - z - i\eta} d\zeta. \tag{11}$$

This function $\mathcal{Z}$ (Eq. 11) can be evaluated as

$$\mathcal{Z}(z) = i\sqrt{\frac{\pi}{2}} \operatorname{erfcx}\left(-\frac{iz}{\sqrt{2}}\right) = i\sqrt{\frac{\pi}{2}} w\left(\frac{z}{\sqrt{2}}\right), \tag{12}$$

where $\operatorname{erfcx}(z)$ is the scaled complementary error function, and $w(z)$ is the Faddeeva function. Other forms exist as well, but those involving multiple terms can suffer badly from numerical instability for $\Im(z) \gg \Re(z)$.

The beam distribution requires more thoughtful treatment. The beam velocity distribution is a generalized Maxwellian with temperature T_b and drift speed $v_b = \sqrt{2E_b/m_b}$ directed at an angle $0° \le \theta_b \le 90°$ with respect to the external magnetic field, where E_b is the beam drift energy. The parallel and perpendicular drift components are thus given as $v_{b\parallel} = v_b \cos\theta_b$ and $v_{b\perp} = v_b \sin\theta_b$, respectively. The beam Larmor radius is defined as $\rho_b = v_{b\perp}/\Omega_b$. The perpendicular drift is uniformly sampled from all directions perpendicular to the external magnetic field, giving the perpendicular distribution function

$$f_{b\perp}(v_\perp) = \frac{1}{2\pi v_{tb}^2} v_\perp \Lambda_0 \left(\frac{v_{b\perp} v_\perp}{v_{tb}^2}\right) \exp\left[-\frac{(v_\perp - v_{b\perp})^2}{2v_{tb}^2}\right]. \tag{13}$$

This function obeys the normalization $2\pi \int_0^\infty f_{b\perp}(v_\perp) dv_\perp = 1$. Note that in the limit $v_{tb} \to 0$, this function converges to the more familiar ring distribution $f_{b\perp} \to \delta(v_\perp - v_{b\perp})$. The distribution function for the beam velocity parallel to the external magnetic field is simply a drifted Maxwellian:

$$f_{b\parallel}(v_\parallel) = \frac{1}{(2\pi)^{1/2} v_{tb}} \exp\left[-\frac{(v_\parallel - v_{b\parallel})^2}{2v_{tb}^2}\right], \tag{14}$$

which obeys the normalization $\int_{-\infty}^{\infty} f_{b\parallel}(v_\parallel) dv_\parallel = 1$. While this beam distribution is likely similar to that of freshly injected beam particles in the C-2U experiment, the beam overall in experiment has a slowing-down distribution, which would tend to blunt the growth of the beam-driven modes examined here.

Substituting f_b into Eq. 4 does not yield closed-form solutions as is the case with the ions and electrons. While the integration over $v_\parallel$ can still be expressed in terms of the $\mathcal{Z}$ function with argument

$$z_{bn} \equiv \frac{\omega - n\Omega_b - k_\parallel v_{b\parallel}}{|k_\parallel| v_{tb}}, \tag{15}$$

the integration over $v_\perp$ has no closed form. These integrals can be evaluated numerically, but can also be expressed as sums over Laguerre polynomials. The tensor $\boldsymbol{\epsilon}_b$ can be expressed compactly as

$$\boldsymbol{\epsilon}_b(\vec{k},\omega) = -\left(\frac{\omega_b}{\omega}\right)^2 \Bigg\{ \boldsymbol{A} + \sum_{n=-\infty}^{\infty} \boldsymbol{B} \circ \left[z_{bn}\boldsymbol{C} + (z_{b0} - z_{bn}\boldsymbol{\mathcal{C}}) \right] \mathcal{Z}(z_{bn}) \Bigg\}, \tag{16}$$

where the $\circ$ operators denotes an element-wise (Hadamard) product. The matrices $\boldsymbol{A}$ and $\boldsymbol{B}$ are given by

$$\boldsymbol{A} \equiv \frac{1}{2} \begin{bmatrix} \alpha_\perp^2 & 0 & -\alpha_\perp^2 \tan^2\theta_k \\ 0 & \alpha_\perp^2 & 0 \\ -\alpha_\perp^2 \tan^2\theta_k & 0 & 2(z_{b0}+\alpha_\parallel)^2 + \alpha_\perp^2 \tan^2\theta_k \end{bmatrix} \tag{17a}$$

and

$$\boldsymbol{B} \equiv e^{-\alpha_\perp^2/2} \begin{bmatrix} \frac{n^2}{\beta_b} & i\frac{n}{\beta_b^{1/2}} & n\frac{z_{bn}+\alpha_\parallel}{\beta_b^{1/2}} \\ -i\frac{n}{\beta_b^{1/2}} & 1 & -i(z_{bn}+\alpha_\parallel) \\ n\frac{z_{bn}+\alpha_\parallel}{\beta_b^{1/2}} & i(z_{bn}+\alpha_\parallel) & (z_{bn}+\alpha_\parallel)^2 \end{bmatrix}, \tag{17b}$$

where $\alpha_{\perp,\parallel} \equiv v_{b\perp,\parallel}/v_{tb}$. The matrices $\boldsymbol{C}$ and $\boldsymbol{\mathcal{C}}$ contain the perpendicular integration, are given by

$$\boldsymbol{C} \equiv \begin{bmatrix} P_n & R_n & P_n \\ R_n & U_n & R_n \\ P_n & R_n & P_n \end{bmatrix} \tag{18a}$$

and

$$\boldsymbol{\mathcal{C}} \equiv \begin{bmatrix} \mathcal{P}_n & \mathcal{R}_n & \mathcal{P}_n \\ \mathcal{R}_n & \mathcal{U}_n & \mathcal{R}_n \\ \mathcal{P}_n & \mathcal{R}_n & \mathcal{P}_n \end{bmatrix}. \tag{18b}$$

The functions that form the elements of these matrices are distinct perpendicular integrals:

$$P_n \equiv \int_0^\infty \xi I_0(\alpha_\perp\xi)\, J_n^2\left(\beta_b^{1/2}\xi\right) e^{-\xi^2/2}\, d\xi, \tag{19a}$$

$$\mathcal{P}_n \equiv P_n - \alpha_\perp \int_0^\infty I_1(\alpha_\perp\xi) J_n^2\left(\beta_b^{1/2}\xi\right) e^{-\xi^2/2}\, d\xi, \tag{19b}$$

$$R_n \equiv \int_0^\infty \xi^2 I_0(\alpha_\perp\xi)\, J_n\left(\beta_b^{1/2}\xi\right) J_n'\left(\beta_b^{1/2}\xi\right) e^{-\xi^2/2}\, d\xi, \tag{19c}$$

$$\mathcal{R}_n \equiv R_n - \alpha_\perp \int_0^\infty \xi I_1(\alpha_\perp\xi) J_n\left(\beta_b^{1/2}\xi\right) J_n'\left(\beta_b^{1/2}\xi\right) e^{-\xi^2/2}\, d\xi \tag{19d}$$

$$U_n \equiv \int_0^\infty \xi^3 I_0(\alpha_\perp\xi) \left[J_n'\left(\beta_b^{1/2}\xi\right)\right]^2 e^{-\xi^2/2}\, d\xi, \tag{19e}$$

and

$$\mathcal{U}_n \equiv U_n - \alpha_\perp \int_0^\infty \xi^2 I_1(\alpha_\perp\xi) \left[J_n'\left(\beta_b^{1/2}\xi\right)\right]^2 e^{-\xi^2/2}\, d\xi. \tag{19f}$$

In the cases of purely perpendicular or parallel propagation ($\theta_k = 90°$ or $\theta_k = 0°$), special care must be taken to re-derive the expressions in Eqs. 7 and 16.

By approximating $\boldsymbol{\epsilon}$, certain closed analytical forms for modes can be found. For this ion beta regime ($\beta = 0.1$), electromagnetic modes, which involve the Alvén speed $v_A = c\left[\sum_\sigma (\omega_\sigma/\Omega_\sigma)^2\right]^{-1/2}$, are highly prominent. In particular, the modes most relevant to this work follow $\omega = kv_A$, while one mode follows $\omega = k_\parallel v_A$ as a variant to this expression. Perhaps the most important simple analytical expression is motivated by Eq. 15: the beam resonance condition, given by

$$\omega = k_\parallel v_{b\parallel} \pm p\Omega_b, \tag{20}$$

where p is an integer. Across various regimes of propagation, this relation will reappear. For $p = \pm 1$, however, the $k = 0$ intercept of this relation is more precisely the hybrid ion resonance[39] at $\omega/\Omega_i = \Omega_b(n_i\Omega_b + n_b\Omega_i)/(n_i\Omega_i + n_b\Omega_b) \approx 1.9$. Because $n_b \ll n_i$ here, this distinction is not of great importance for the mode structure.

More generally, however, Eq. 1 must be solved numerically, particularly for cases where the entire dielecic tensor is needed to produce the examined modes, such as will be seen in the case of near-perpendicular propagation. Indeed, while simulations are the primary tool for this study, numerical solutions to Eq. 1 help to further clarify and complement the results from simulations. Following this logic, numerical (semi-analytical) methods were used in this work to confirm and better understand the simulation results.

Equation 1 can be solved numerically for choice of plasma parameters and the angles θ_k and θ_b. To do so, a 2D grid of real (ω) and imaginary (γ) frequencies and a list of k values for the relevant physics are first defined. For each k value, each box in the frequency sample grid is mapped as a contour through the dispersion function, and the winding number of the resultant mapping indicates whether a solution is present. In most cases, the

beam density is lowered to 10% of that of the simulation beam density to ensure that the semi-analytical growth rate remains in the linear regime, $|\gamma| \ll |\omega|$. Generally the mode structure is not strongly affected by this consideration. The linear dispersion relation, polarization and growth or damping rate for a wave mode for arbitrary propagation and beam injection angle can thus be determined. Because this technique can produce many solutions along cyclotron resonance cones, certain of these solutions may be omitted for clarity.

III. KINETIC SIMULATION OF IC WAVES

Particle-in-cell (PIC) simulations can, in a sense, serve as an exact solver for the types of linear waves excited in a plasma and their nonlinear coupling and evolution over time. Examining the exemplary case of the observed fusion enhancement in the C-2U experiment, we model IC waves in the C-2U SOL environment, corresponding to a radius of about 45 cm. The near-uniform axial magnetic field in the SOL readily allows dissection of the important physics. We demonstrate the main kinetic dynamical processes via a PIC simulation with one spatial dimension and three velocity dimensions using the electromagnetic particle simulation code LSP[40]. The SOL plasma is modeled as a locally homogeneous deuterium and electron plasma with a proton beam in a uniform (axial) magnetic field. Each is designated with the subscripts i, e, and b, respectively, and σ designates an arbitrary species. We will also briefly consider the case of a boron-11 (B^{11}) thermal plasma with hydrogen beam. The spatial dimension of the simulation is labeled the $\hat{x}$ direction. The external magnetic field is given a strength of $B_0 = 750$ G and is directed at an angle $0° \leq \theta_k \leq 90°$ with respect to the x axis to define the direction of the wavevector $\vec{k}$. A schematic representation of the simulation geometry is shown in Fig. 1.

The ions and electrons are given a temperature of $T_{i,e} = 200$ eV, and the beam is given $T_b = 500$ eV. All temperatures are isotropic; instabilities deriving from anisotropic temperature are not considered here (except in the sense that a beam population adds velocity anisotropy). The beam drift energy is $E_b = 15$ keV. The plasma component densities n_σ are defined relative to the ion density $n_i = 7 \times 10^{18}$ m^{-3}. The beam density is 10% of this value: $n_b = 0.1 n_i$, and the electron density is determined by these two quantities to preserve quasineutrality.

Because the relevant length scale is that of ion cyclotron motion (ρ_i), which for the SOL environment is taken here to be much larger than the Debye length λ_D, an implicit algorithm is adequate[41], allowing a grid spacing $\Delta x \gg \lambda_D$. In particular, the size and resolution of the spatial domain are such that the modes of interest are well-resolved in k space and the total domain size is much larger than the relevant mode wavelength to prevent waves deriving solely from the periodic boundary

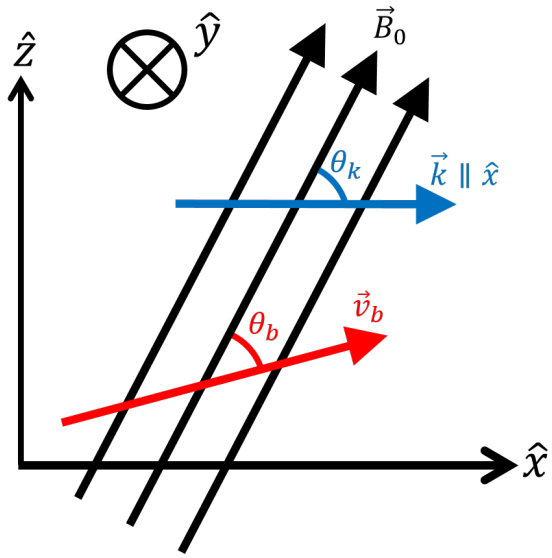

FIG. 1: A schematic representation of the 1D PIC simulation geometry. The one degree of spatial freedom is taken as the $\hat{x}$ direction, with the external magnetic field $\vec{B}_0$ oriented in the x, z plane at an angle θ_k with respect to $\hat{x}$ to define the angle of wave propagation. The beam population is given perpendicular and parallel components with respect to $\vec{B}_0$ according to the angle θ_b.

conditions. The timestep Δt resolves all major frequencies lower than the plasma frequency ω_p, including the ion plasma frequency ω_i and the electron cyclotron frequency Ω_e), but we only concern ourselves with frequencies approximately $\omega \leq 10\Omega_i$. To further assist with the timestep, the electrons are given a mass of 20 times their realistic mass, with care taken to ensure than doing so does not discernibly affect mode structures and growth rates. Because the collision timescale is much longer than the ion cyclotron timescale, collisions are neglected.

To analyze the mode structure of the waves in the simulation, a 2D FFT over the spatial and temporal dimensions of the perturbed fields is taken to give $\delta\vec{E}(k,\omega)$ and $\delta\vec{B}(k,\omega)$ in Cartesian polarizations. From these the circular polarizations are calculated, with handedness defined such that a right-handed mode circulates in the same direction as an electron, and a left-handed mode circulates in the same direction as an ion, regardless of propagation direction. From the 1D nature of the simulation, $\delta B_x = 0$ to ensure $\vec{\nabla} \cdot \vec{B} = 0$. Consequently, δB_z solely represents the magnetically compressional component of waves. To isolate the compressional component of the electric field, however, the fields must be rotated. Additionally, as $\hat{y} \perp \vec{B}_0$, δB_y always represents the magnetically shear component of waves. Meanwhile, E_x represents the electrostatic (longitudinal) component of waves. While only the electric field can do work on ions, for the ion beta in this case ($\beta = 0.1$), it should be noted that

the magnetic energy content of these waves dominates the electric energy content. For the purposes of the dispersion plots that follow in this paper, $|\vec{k}| \geq 0$, with $\omega < 0$ representing backwards propagation. While an alternative scheme where ω is kept positive and $\vec{k}$ is allowed to be reversed would also suffice, the present convention will aid in the illustration of mode structure in some instances.

IV. IC WAVES PROPAGATING PARALLEL TO THE MAGNETIC FIELD

To begin the scan over angular parameters θ_k and θ_b, first consider the regime of wave propagation parallel (or nearly parallel) to the external magnetic field, $\theta_k \approx 0°$. In contrast to the case of perpendicular propagation, here only the cyclotron fundamentals $\omega = \pm\Omega_\sigma$, as well as an unmagnetized contribution, enter into the dispersion relation. Discounting the plasma oscillation, this regime is the domain of three chief modes: two shear Alfvén modes and the ion acoustic mode, which in this regime obeys $\omega = kv_s$, where $v_s = \sqrt{(T_e + 3T_i)/m_i}$ is the ion sound speed. While the former two modes are transverse and have shear polarizations, the latter is electrostatic (longitudinal). However, in the present parameters ($v_s < v_A$), the ion acoustic mode is strongly damped and is not of concern. In contrast, the shear Alfvén modes are potentially excitable.

These two transverse modes are circularly polarized, one right-handed and the other left-handed. At low frequency, $\omega \ll \Omega_i$, both branches obey $\omega = v_A k$, but begin to diverge once ω approaches Ω_i. The right-handed branch thus does not resonantly couple to ions and passes through Ω_i unimpeded. The mode in this frequency regime is termed a Whistler[42] before finally resonating the electrons at $|\Omega_e|$. In contrast, the left-handed branch cannot pass through Ω_i and instead resonates with ions. This mode is thus termed the Alfvén-ion-cyclotron (AIC) mode[31] and can be excited by a temperature anisotropy in the ions[4]. In mirror machines, such a mode can lead to scattering of ions into the loss cone. In a plasma composed of only thermal ions and electrons with purely parallel propagation ($\theta_k = 0°$), the mode structure is shown in Fig. 2 where the right- and left-handed components are distinguished. The resonance of the AIC mode with the ion cyclotron resonance cone $\omega - \Omega_i = kv_{ti}$ is visible.

With the addition of an energetic beam population, either of these shear modes can become excited depending on the beam injection angle, which in turn determines the beam resonance condition (Eq. 20). Figure 3 shows the case of purely parallel propagation and beam injection ($\theta_k = \theta_b = 0°$) with the beam resonance lines indicated. As a consequence of the purely parallel propagation, only the $p = \pm 1$ beam resonance lines enter into the dispersion relation. Purely parallel beam injection then causes these resonance lines to have their maximum possible slope. With the present beam energy, these conditions

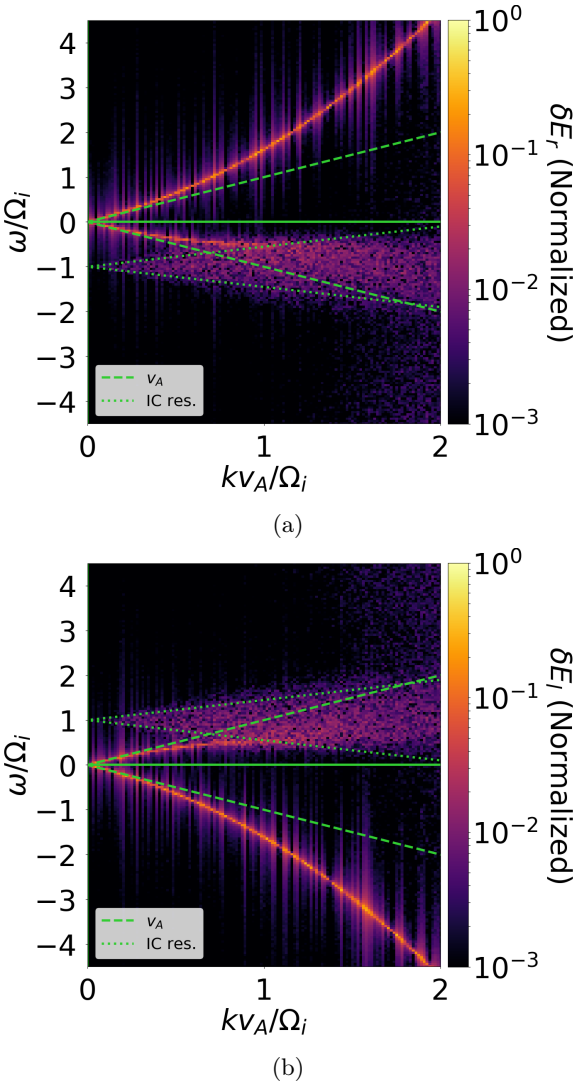

(a)

(b)

FIG. 2: Dispersion relations for right-handed (2a) and left-handed (2b) components of the electric field for purely parallel propagation ($\theta_k = 0°$) and no beam population. Frequency is normalized with respect to the background ion (deuterium) cyclotron frequency Ω_i, and the wavevector is normalized with respect to v_A/Ω_i. The space where $\omega < 0$ indicates backwards propagation. The intensity at a particular mode is indicated by the heat-map and is normalized with respect to the maximum value. The Alfvén velocity $\omega = kv_A$ is indicated as a dashed line. The dotted lines bound the approximate cone of strong ion cyclotron damping, $\omega = 2kv_{ti}$.

cause the $p = -1$ line to excite the right-handed mode in the forward direction, and, to a lesser extent, the left-handed mode in the backward direction, both at roughly $|\omega| \approx \Omega_i$. There is also a mode associated with the beam resonance lines themselves, for which the $p = +1$ line is left-handed, and the $p = -1$ line is right-hand. Interestingly, the $\omega < 0$ portion of the right-handed waves are

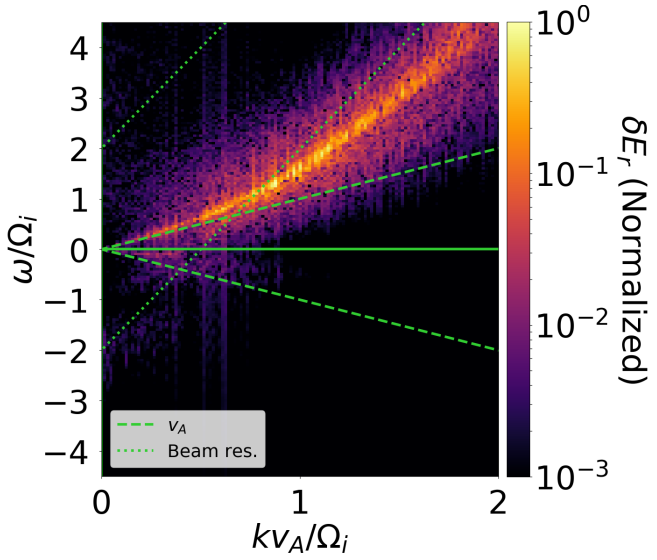

(a)

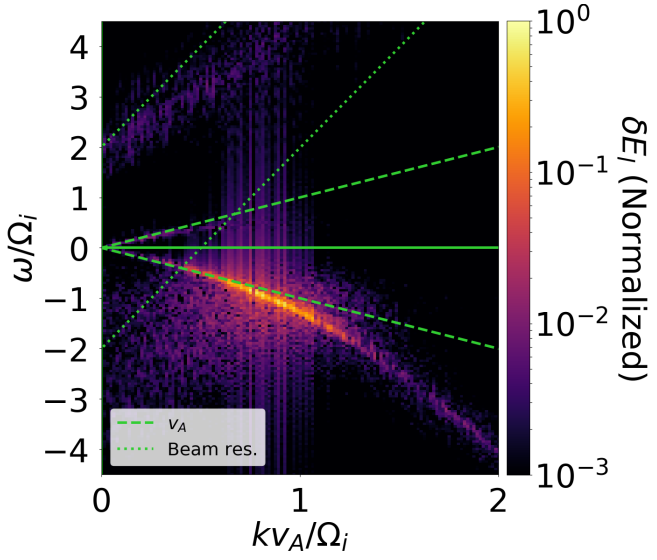

(b)

FIG. 3: The dispersion relation for right-handed (3a) and left-handed (3b) components of the electric field for purely parallel propagation ($\theta_k = 0°$) and a purely parallel-streaming beam population ($\theta_b = 0°$). The beam resonance lines for $p = \pm 1$ in Eq. 20 are indicated with dotted lines.

also bent "into line" with the $p = -1$ resonance, crossing $\omega = 0$. The right-handed excitations bear resemblance to the right-hand resonant and non-resonant modes studied previously[27,28]. The excitation of the right-handed mode with $\omega > 0$ is extremely robust and may lead to inefficient but finite coupling to ions, as an increase in the ion perpendicular temperature to 275 eV is produced in this case. It is also possible that the much smaller left-handed excitations may be producing this warming, which could do so much more efficiently.

The effect of the beam population on the dispersion relation for parallel beam injection can be more clearly seen by solving for the linear waves numerically as outlined in section II. The output of this numerical solving method is shown in Fig. 4 for $\theta_k = \theta_b = 0$ and $n_b/n_i = 0.01$. The points of the dispersion relation are colored according to growth or damping rate, as is indicated in the color bar. The red points indicate growth (instability), and the blue points indicate damped modes. Grey indicates marginal stability. In addition to the instability expected along the right-handed mode for $\omega > 0$, this plot also shows that the $\omega < 0$ portion of the right-handed branch is strongly affected by a resonance with the beam resonance line for $p = -1$ in Eq. 20. For numerical stability, the smallest wavevector treated is $kv_A/\Omega_i = 0.1$, and the smallest real frequency treated is $\omega/\Omega_i = 0.09$. Cyclotron resonance cones are visible at $\omega/\Omega_i = \pm 1$.

For near-perpendicular beam injection, the excitation shifts predominantly to the backward-propagating right-handed mode, as is shown in figure 5 for $\theta_b = 75°$, but is much less robust than in the case of parallel beam injection. This mode generates similar bulk heating as in the previous case, however. If the beam injection angle is increased further to $\theta_b = 90°$, mode activity diminishes greatly, the beam resonance lines coupling poorly with both shear Alfvén modes. Instead, the dominant mode activity falls along the beam resonance lines themselves at the hybrid ion resonance[39] at $\omega/\Omega_i \approx 1.9$. This mode is left-hand polarized for $\omega > 0$ and right-hand polarized for $\omega < 0$.

In both of these cases, a significant portion of the wave activity driving ion acceleration occurs for phase velocities within reach of the ion thermal distribution, particularly for perpendicular beam injection. The resulting increase in perpendicular temperature opens the possibility of the AIC instability caused by temperature anisotropy, and in a mirror (or FRC SOL) situation could lead to scattering of ions into the loss cone. In the C-2U experiment, the beam injection angle is close to $\theta_b = 75°$, and so the near-perpendicular injection case examined here likely presents a closer picture to the experimental reality. However, evidence of such modes has not been seen in this experiment, suggesting that either the dominance of other modes or that the resultant perpendicular heating is too subtle to observe.

V. IC WAVES PROPAGATING OBLIQUELY TO THE MAGNETIC FIELD

If the angle of wave propagation is increased, the circularly polarized shear modes and ion acoustic mode explored in the previous section gradually transition into linearly polarized shear and compressional Alfvén modes. The former mode follows $\omega = k_\parallel v_A$ and is restricted to $\omega < \Omega_i$. This mode can therefore not propagate if $\theta_k = 90°$. The latter mode follows $\omega = kv'_A$ in the limit of long wavelengths (as is relevant to this work), where

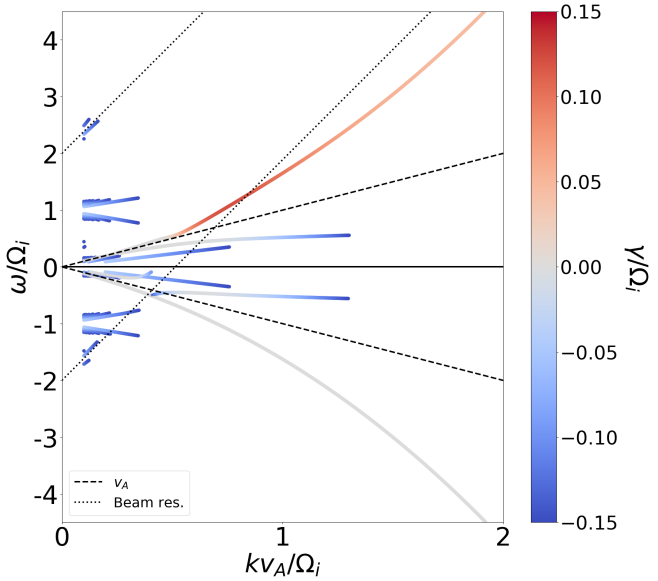

FIG. 4: The dispersion relation for the real frequency ω from numerical solution of Eq. 1 for $\theta_k = \theta_b = 0$ and $n_b/n_i = 0.01$ for a hydrogen beam and deuterium plasma, corresponding to Fig. 3. The color scale indicates the imaginary part of the frequency γ. Red indicates growth (instability), and blue indicates damping. Grey indicates marginal stability. The dashed lines indicate the Alfvén speed, and the dotted lines indicate the beam resonance condition for $p = \pm 1$ in Eq. 20.

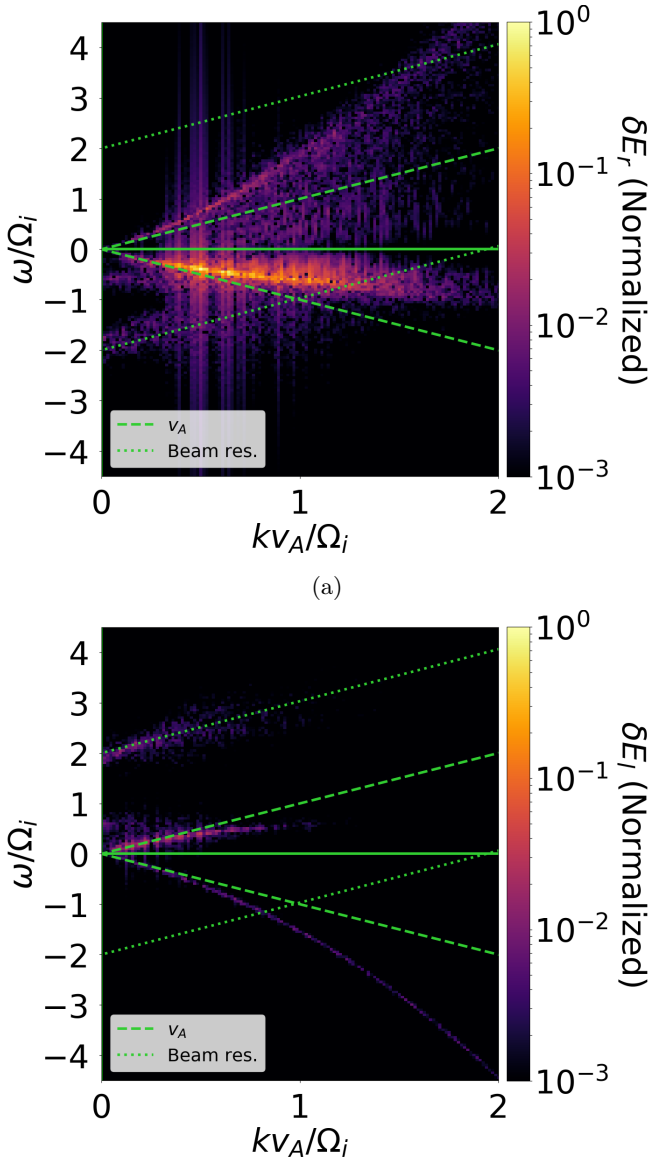

FIG. 5: The dispersion relation for right-handed (5a) and left-handed (5b) components of the electric field for purely parallel propagation ($\theta_k = 0°$) and nearly perpendicularly injected beam population ($\theta_b = 75°$).

$v'_A = \sqrt{v_A^2 + v_s^2} \approx v_A$ in this parameter regime, and converges to the lower-hybrid frequency ω_{LH} for short wavelengths. This mode is called variously the magnetoacoustic, magnetosonic, or extraordinary mode.

The details of this evolution are partially determined by the ion sound speed v_s. If $v_s > v_A$, the ion acoustic mode migrates to the new phase velocity v'_A and adopts a magnetically compressional polarization while the right-handed shear mode "wilts", shifting to follow $\omega = k_\parallel v_A$ and becoming strongly damped. Conversely, if $v_s < v_A$, the right-handed shear mode shifts to the phase velocity v'_A and becomes a compressional mode while the ion-acoustic mode "wilts", following $\omega = k_\parallel v_s$ and inevitably becoming more strongly damped. In the present parameter regime, the latter case prevails, and as $v_s \ll v_A$, we hereafter take $v'_A = v_A$.

In addition to its magnetically compressional character, the compressional mode possesses a hybrid electric character, having both a longitudinal and transverse component. This longitudinal component will prove highly effective at generating a fast ion tail, as is explored in section VI. However, the shear mode also possesses a longitudinal electric component, which for $\theta_k < 90°$ may generate ion heating.

For $\theta_k \approx 90°$, the compressional mode features resonances with ion-Bernstein harmonics, particularly those of the beam population. In this section, however, our interest is the mode structure for $\theta_k \approx 60°$, where the Alfvén modes become dominantly linearly polarized, but without ion-Bernstein resonances. The mode structure without a beam population is shown in figure 6. Some of the remnants of the parallel-propagation mode structure can be seen, such as in the slight upward or downward curvature of the compressional mode for $\omega > 0$ and $\omega < 0$, respectively.

The addition of the beam population excites these base modes. In this parameter regime, the excitation is comparable between the compressional and shear modes, as

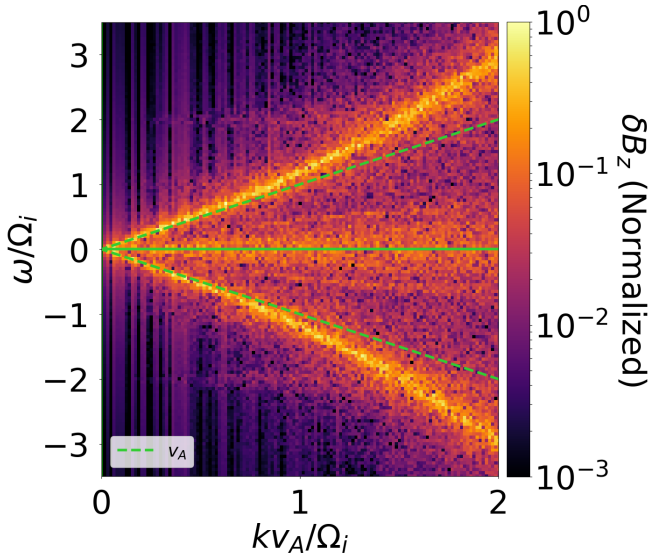

(a)

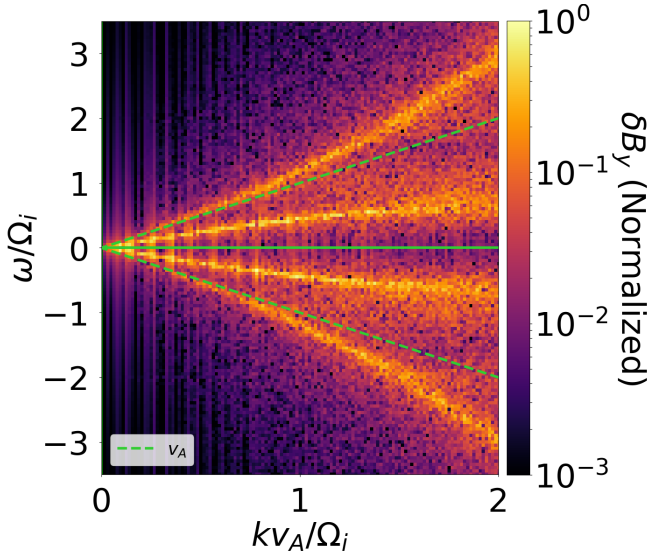

(b)

FIG. 6: The dispersion relation for the compressional (6a) and shear (6b) components of the magnetic field for oblique propagation ($\theta_k = 60°$) and no beam population.

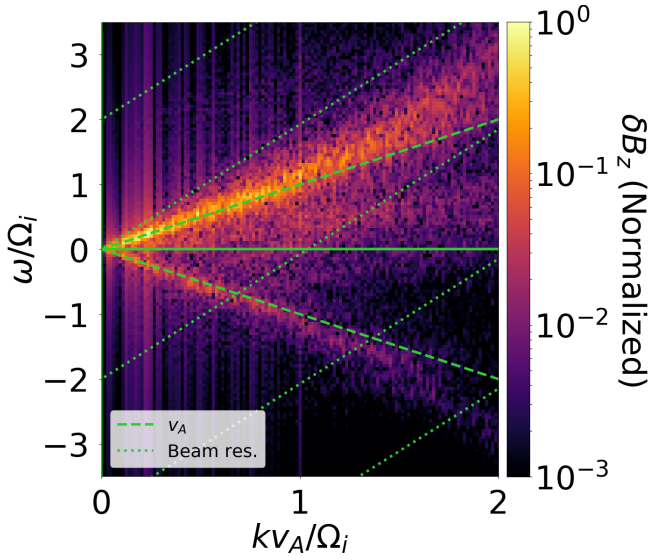

(a)

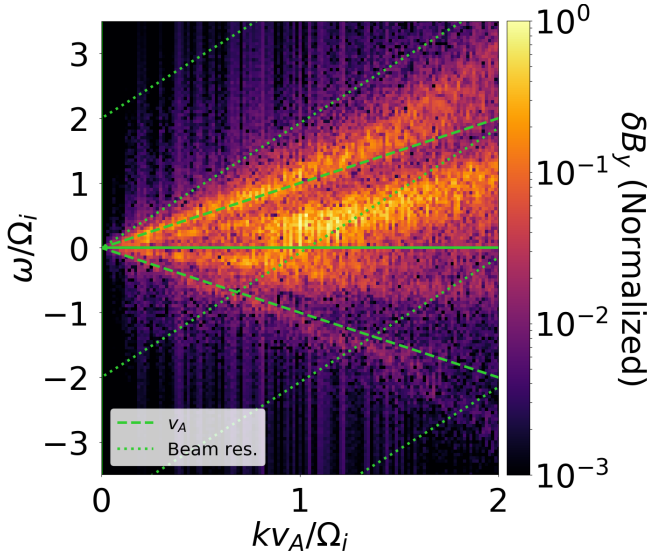

(b)

FIG. 7: The dispersion relation for the compressional (6a) and shear (6b) components of the magnetic field for oblique propagation ($\theta_k = 60°$) and a beam population injected at $\theta_b = 15°$. All available harmonics of the beam resonance condition (Eq. 20) are shown.

is shown in figure 7 for $\theta_k = 60°$ and $\theta_b = 15$. For near-perpendicular beam injection, the mode activity generally diminishes and shifts to a compressional mode that may be due to the $p = 0$ beam resonance line. In the the former case, substantial perpendicular bulk heating of the ions occurs, with the perpendicular ion temperature approximately doubling. In the latter case, there is essentially no heating of background thermal ions.

VI. IC WAVES PROPAGATING PERPENDICULAR TO THE MAGNETIC FIELD

In the regime $\theta_k \approx 90°$, cyclotron harmonics, typically in the form of ion-Bernstein modes, assert themselves over the continuum modes of the previous section. The cyclotron motion of the ions causes significant dispersion in the otherwise Alfvénic mode structure. As these modes are typically electrostatic (longitudinal) in nature, electrostatic physics with regard to wave-particle coupling becomes particularly important. The case of

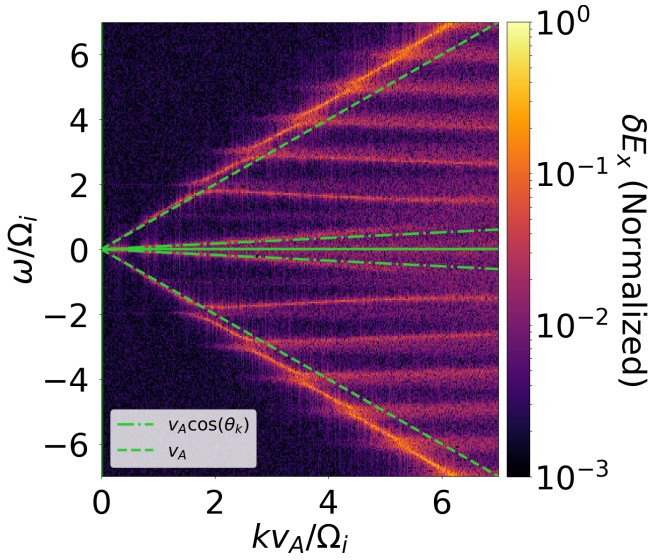

FIG. 8: The dispersion relation for the longitudinal (electrostatic) component for near-perpendicular propagation ($\theta_k = 85°$) without a beam population.

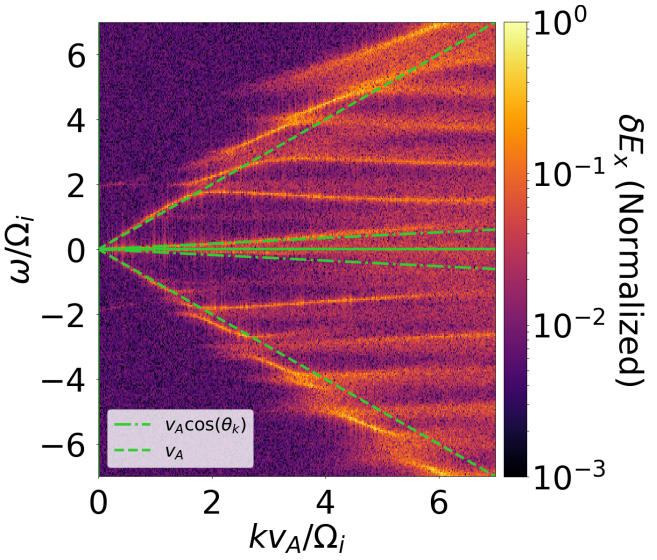

FIG. 9: The dispersion relations for the electrostatic component for near-perpendicular propagation ($\theta_k = 85°$) and a beam population injected at $\theta_b = 0°$.

purely perpendicular propagation is not examined because both mode excitation and wave-particle coupling tend to be poor. A small but finite $k_\parallel$ typically makes a dramatic difference. The mode structure for the near-perpendicular regime $\theta_k = 85°$ is shown in figure 8. The compressional mode forms the spine of the wave activity, but resonances with the even cyclotron harmonics can now be seen in the form of ion-Bernstein modes, in contrast to the case of the previous section. These resonances are greatly amplified by the presence of a beam population and create ion acceleration of sufficient interest that the nonlinear interaction of these modes with the background ions is given a separate subsection.

A. Linear Physics: Beam-Driven Ion-Bernstein Modes

When a beam population is added to the plasma, the mode structure in figure 8 is modified in distinct ways depending on the beam injection angle. These differences broadly manifest according to the relevance of the cyclotron motion of the beam ions. For purely parallel injection, the only beam cyclotron motion is due to finite temperature. Thus, the background ions dictate the IC mode structure. The case of perpendicular waves driven by a streaming population has been investigated extensively[5,6,10–13], though mostly in a low-beta regime. In such a regime, many cyclotron harmonics are excited with the mode growth rate broadly monotonically decreasing for higher harmonics. The excitations, while sharp in frequency space, are spread over a large range in k at essentially constant frequency. In the present case, however, where $\beta = 0.1$, the electromagnetic contribution is substantial, as is shown in figure 9 for $\theta_k = 85°$ and $\theta_b = 0°$. Notably, the first few harmonics are modified by an excitation of the shear Alfvén mode. The excitation of these modes is remarkably weak compared with the other regimes examined, and as a partial consequence produce weak ion heating. Of course, the principle of heating plasma by injection of a streaming species is well-established but may be less effective with regard to collective effects in a high-beta regime.

In the opposite regime, that of near-perpendicular beam injection, the magnetoacoustic instability may be excited, as has been investigated previously[17–20,43]. The exemplary case of $\theta_k = 85°$ and $\theta_b = 75°$ is shown in figure 10 for both the numerically solved dispersion relation and that found from PIC simulation. Both approaches are in agreement, with the former providing sharper detail of the intricate mode structure and the latter emphasizing the resonance locations. Cyclotron resonance cones are still visible for the numerical solution, but have been generally suppressed for clarity. The intersections of the beam resonance lines and the compressional mode determine the dominant excitations. Because both $k_\parallel$ and $v_{b\parallel}$ are finite, Doppler shifting causes the resonant points to deviate from the pure beam cyclotron harmonics. For the angular parameters use in figure 10, the result is a summation of harmonics in the positive propagation direction and a dominant first beam cyclotron harmonic in the backwards propagation direction. In real space, the electrostatic component of this mode structure manifests as coherent, periodic sharp peaks propagating in the forward direction that ride atop a backwards-propagating sinusoidal wave. The fundamental frequency for both is approximately the beam cyclotron frequency, $\omega = 2\Omega_i$. Additionally, because the phase velocity of this mode is much faster than the ion thermal speed ($v_A/v_{ti} \approx 4$),

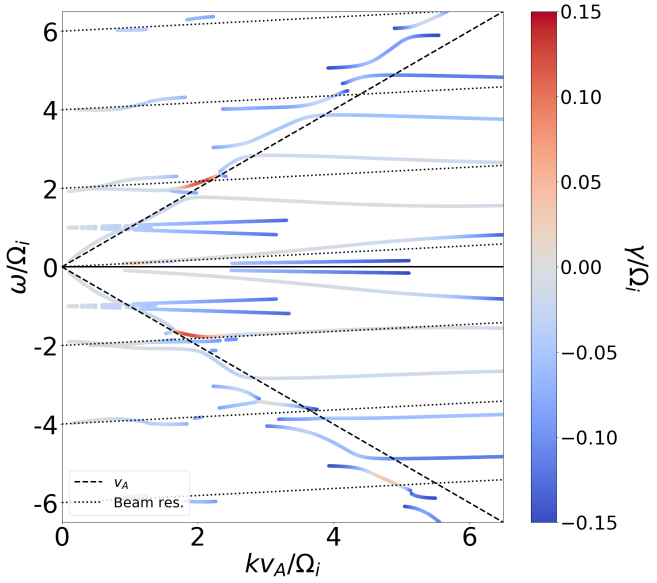

(a)

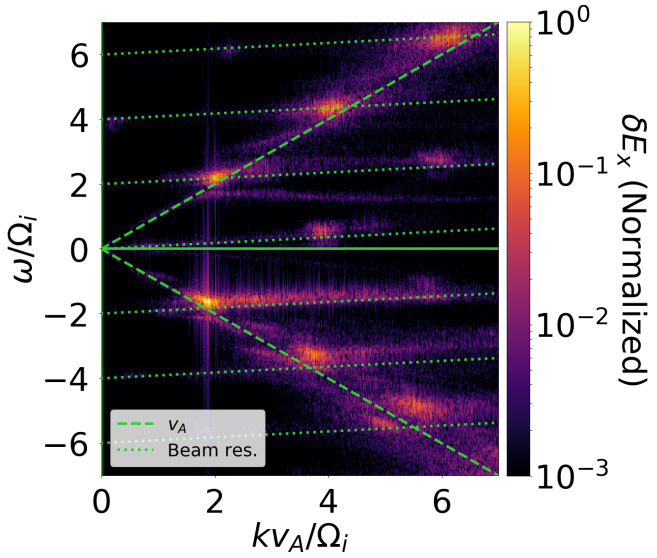

(b)

FIG. 10: The dispersion relations for the electrostatic component for near-perpendicular propagation ($\theta_k = 85°$) and a beam population injected at $\theta_b = 0°$. The top plot (Fig. 10a) shows the numerical solution of Eq. 1, and the bottom plot (Fig. 10b) shows the equivalent dispersion relation from PIC simulation. Here, both cases use the same beam density ($n_b = 0.1n_i$) and are overlaid with all available harmonics of the beam resonance condition (Eq. 20).

there is little coupling to the bulk motion of ions[9]. This field configuration is highly amenable to allowing the nonlinear generation of a fast-ion tail. This electrostatic component of the mode also produces density fluctuations in the plasma with an essentially identical mode structure.

B. Nonlinear Physics: Wakefield Acceleration of Ions

The fast phase velocity $v_{ph} = v_A \gg v_{ti}$ of the magnetoacoustic mode shown in figure 10 allows the mode saturation level to depart from that predicted by quasilinear theory. Instead, the waves grow until reaching a robust saturation without strong damping on the bulk plasma. The ionic wave trapping velocity[37] $v_{tr} = \sqrt{q_i E/m_i k}$, where E is the electric field of the wave and k is the mode wavevector, grows with the wave amplitude until reaching nearly the wave phase velocity. The corresponding wave saturation level is the Tajima-Dawson field[36] $E_s = m_i \omega v_{ph}/q_i$ commonly encountered in wakefield acceleration. In the present case, where the mode frequency approximately corresponds to an integer multiple n of the ion cyclotron frequency and $v_{ph} = v_A$, this expression becomes[9]

$$E_s(n) = nB_0 \frac{v_A}{c}. \tag{21}$$

The wave can then begin damping on the fastest thermal particles, accelerating them to much higher energies. The saturation level from simulation is approximately 60% of the value predicted by $E_s(2)$, owing to the finite value of v_{ph}/v_{ti}. In supplemental runs where the ions are initialized with a colder temperature, raising this ratio, the saturation level indeed converges to that predicted by Eq. 21 for $n = 2$.

Because the electrostatic field of this mode is directed nearly perpendicularly to the external magnetic field, the wave cannot significantly displace ions from their starting gyro-center, instead merely kicking them into a larger cyclotron orbit. This effect, in combination with the high phase velocity of the mode, results in the generation of a large tail of fast ions without an increase in the bulk temperature of the ions or induced transport, drifts, or turbulence. The acceleration is chiefly in the perpendicular velocity direction, but because the overall temperature is not significantly increased, instabilities from anisotropic temperatures are avoided. Additionally, because the mode frequency is an integer multiple of the ion cyclotron frequency, cyclotron acceleration allows an accelerated ion to be periodically recaptured by the wave, increasing the efficiency of acceleration and propelling ions to energies up to the beam energy E_b.

The result of this fast-ion tail is a dramatic increase in the D-D fusion power. Letting P_{th} be the initial thermonuclear D-D fusion power and P be the fusion power at a later time, the present mode generates $P/P_{th} > 10^4$, providing a possible explanation for the anomalously high neutron rate seen in the C-2U experiment[8]. Indeed, these angular parameters seem to produce the maximum potential for fusion enhancement. Figure 11 shows the fusion enhancement across the full range of angular parameters scanned in this work, indicating a strong peak for approximately $\theta_k = 85°$ and $\theta_b = 75°$. While the mode excitation in other regimes is potentially far more robust, even a relatively small excitation in this regime

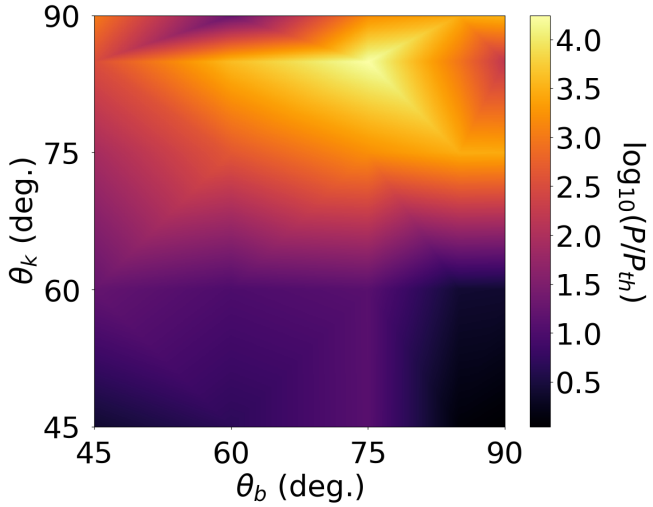

FIG. 11: The maximum fusion enhancement P/P_{th} for a scan over angular parameters θ_k (vertical axis) and θ_b (horizontal axis). Each angular parameter is sampled in mostly 15° increments but also includes 5° and 85°. The bright peak in the upper right corner corresponds to $\theta_k = 85°$ and $\theta_b = 75°$, which was used in generating figure 10.

of angular parameters has far more potential for fast-ion generation.

While the ions strongly interact with the wave in this fashion, the electrons see an essentially static field and respond adiabatically. The electrons briefly experience an $\vec{E} \times \vec{B}$ drift given by $\vec{v}_{EB} \approx -2v_A\hat{y}$ as each wave passes. Such a mean shift in the electrons (by $2v_A/v_{te} \approx 0.6$) is indeed seen in the simulation following the wave peaks. Furthermore, because the electrons respond together in this drift, the mean of the electron v_y distribution merely shifts by v_{EB}; turbulence is not created.

The growth of this mode also deviates from the usual picture of quasilinear physics. In such a model, a positive slope in the velocity distribution function ($\partial f/\partial v > 0$) provides free energy for the wave to grow. More particles are decelerated by the wave than accelerated, and the region of positive slope flattens. In the present case, however, consider the total distribution of beam and thermal ions, the phase velocity v_A lies within a region where $\partial f(v_x)/\partial v_x < 0$, and indeed the mode can still grow exponentially even with warmer ions, reinforcing the negative slope at the phase velocity. The resolution of this situation is that the free energy is coming not from a driver at the phase velocity, but rather at the beam velocity, which has $v_b \gg v_A$. The coupling of the beam resonance with the compressional mode allows the free energy of the beam to be channeled into a wave with phase velocity $v_{ph} = v_A$. The beam population contains sufficient such free energy to drive an exponentially growing mode even in a region of velocity space that is quasilinearly stable. The mode then grows until saturating via Tajima-Dawson wakefield physics. The population of fast beam particles then remains as a reservoir of free energy for the mode. Over the course of a simulation, the beam population gradually loses energy to the mode and thermal plasma, until the free energy is depleted, causing the mode to dissipate.

Another distinction from typical quasilinear saturation is in the realm of saturation through coupling to other modes. Some considerations suggest that such a mechanism does not play a substantial role in the present case. First, the excitation of higher beam cyclotron harmonics is a fundamental feature of this particular mode and, in this case, coherently add together. Rather than dissipating energy, the higher harmonics merely increase the sharpness of the waveform until the wakefield saturation level is reached. This conclusion is further strengthened by the supplemental simulations with a colder ion population, suggesting that the relationship between the wave phase velocity and ion thermal speed are the crucial factors determine the saturation amplitude. If dissipation through higher harmonics occurs, it does not seem to appreciably affect the saturation level in this case.

VII. ENHANCEMENT FROM BEAM BUNCHING

The fast-ion tail generated by this mode is potentially beneficial for efforts at fusion energy. The benefit and efficiency of this process may be even further increased if this mode is excited directly, without needing to grow spontaneously from noise from the free energy provided by the beam. A potential means of doing so is indicated by the beam and ion density fluctuations also excited by the electrostatic component of this mode, similar to the self-modulation instability in ion-driven wakefield acceleration[44–46], where an injected ion beam becomes bunched at the plasma wavelength, improving wakefield development. Seeding the beam density with bunches[47] with the same wavelength as that of the mode could thus immediately and robustly excite the mode, akin to playing a musical instrument at a particular note.

If the beam density is seeded with square wave bunches with period $\lambda_b = \pi v_A/\Omega_i$, corresponding to the fundamental resonance of the mode at $\omega = 2\Omega_i$, such an effect is indeed seen. The fundamental resonance at $\omega = 2\Omega_i$, as well as its higher beam harmonics, become sharply dominant in the dispersion relation, and the real-space structure of the mode becomes more robust, consistent, and coherent. Additionally, a significant boost to the fusion rate growth is also seen, likely a result of this cleaner mode structure.

To further examine the benefit to fusion rate from beam bunching, the exemplary run with $\theta_k = 85°$ and $\theta_b = 75°$ is repeated for a scan of beam velocity values in the range $v_b/v_{ti} \in [4, 128]$. Concerns of numerical stability define the upper limit. The cases of no bunching, bunching corresponding to the resonance at $\omega = 2\Omega_i$, and bunching corresponding to $\omega = \Omega_i$ at each beam velocity are treated. The maximum D-D fusion rate normalized

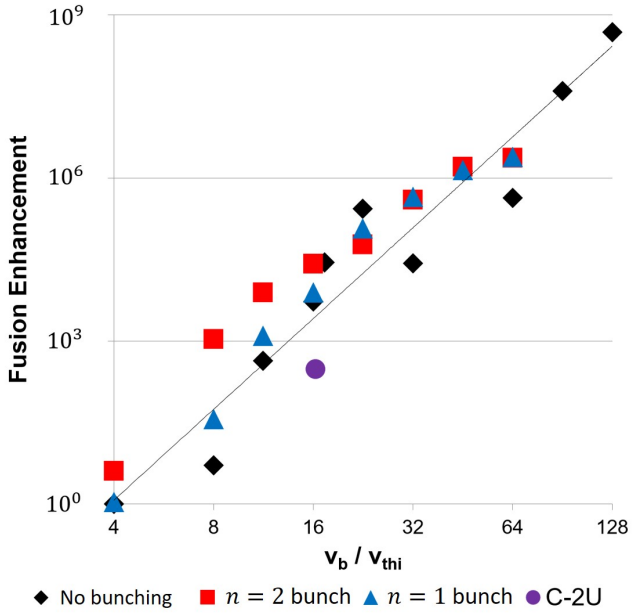

FIG. 12: The maximum D-D fusion rate normalized to the initial thermonuclear rate for various beam velocities for the case $\theta_k = 85°$ and $\theta_b = 75°$. Black points have no beam bunching; red points, bunching at $\lambda_b = \pi v_A/\Omega_i$, corresponding to the resonance at $\omega = 2\Omega_i$; and blue points, bunching at $\lambda_b = 2\pi v_A/\Omega_i$, corresponding to $\omega = \Omega_i$. The purple point is the approximate position of the observed fusion enhancement in the C-2U experiment.

to the initial thermonuclear rate in each run is then tabulated in figure 12 and compared with the approximate result from the C-2U experiment. The singular case considered previously roughly corresponds to $v_b/v_{ti} = 16$.

The points with no bunching indicate a power-law relationship in the fusion enhancement of approximately $P/P_{th} \propto (v_b/v_{ti})^{5.6}$ at this ion temperature. With bunching corresponding to the mode at $\omega = 2\Omega_i$, there is a further enhancement of fusion power over the unbunched case for $v_b/v_{ti} \lesssim 16$. In the same range, the fusion enhancement from bunching corresponding to $\omega = \Omega_i$ for comparison is indistinguishable from the unbunched case. This result makes sense. Not lying along a beam resonance line, $\omega = \Omega_i$ is not spontaneously excited in the un-bunched case, and so attempting to do so with bunching effectively produces inaccessible free energy. This example demonstrates the importance of choosing the correct mode at which to bunch the beam; with Doppler-shifting of frequencies caused by finite $k_\parallel$ and $v_{b\parallel}$, this effort may be nontrivial in some cases.

For the higher range of beam velocities, $v_b/v_{ti} \gtrsim 16$, bunching at both $\omega = \Omega_i$ and $\omega = 2\Omega_i$ converges in the resulting fusion enhancement. This departure from the lower-energy beam regime is likely a result of a change in the excited mode structure for beams of such energy. Rather than the ion-Bernstein resonances as in the case of figure 10, the $n = 0$ beam resonance mode become dominant. As this mode has $\omega < \Omega_i$ and lies along a continuum, bunching at all harmonics $\omega = n\Omega_i$ may becomes equivalently ineffective. Nonetheless, for the regime considered in the C-2U experiment, bunching of the beam population, perhaps by pre-exciting the magnetoacoustic mode with a uniform beam or with RF techniques, may allow a systematic increase in fusion efficiency. Here, knowledge from the field of plasma accelerators may be of significant assistance.

VIII. ANALOGY TO A PROTON-BORON-11 PLASMA

One of the ultimate goals of the successor experiments of C-2U is to achieve a burning proton-boron-11 plasma (pB^{11}). It is thus worthwhile to briefly consider how the physics examined thus far for a deuterium plasma and proton beam applies to this case. The B^{11} (the a fully ionized charge of +5) is treated as the background plasma, and the protons are treated as the beam. Compared to the previous cases then, essentially the only change is that the background ion species is swapped for boron-11, with the electron density increased to preserve quasineutrality.

With the aim of reproducing the favorable fast-ion tail generation seen for a deuterium plasma for $\theta_k = 85°$ and $\theta_b = 75°$, an intuitive comparison of B^{11} and deuterium may suggest that both should yield similar physics, as the cyclotron frequencies are nearly identical, as well as the ratio of Alfvén speed to ion thermal velocity. While q_i/m_i is nearly the same in both cases, however, the species plasma frequencies ω_i are distinct, owing to the +5 charge of B^{11}. With the subscripts B and D respectively denoting B^{11} and deuterium, $(\omega_B/\omega_D)^2 = 5$. Linear theory (Eq. 4) then dictates that this squared ratio boosts the contribution of the background ions in the plasma dielectric tensor and is effectively equivalent to lowering the density of the beam population. Consequently, the resonances of the compressional mode and beam resonance lines seen in figure 10 are muted, and the magnetoacoustic instability is overall much less robust.

Instead, electrostatic activity is found more robustly in the slightly more oblique propagation regime considered in section V. An example case is shown in figure 13. The excitation broadly falls along the compressional Alfvén mode. In real space, this mode structure manifests as a wave two length scales: a smaller wavelength corresponding to roughly $\lambda = \pi v_A/\Omega_i$ and a longer length (about 5λ) over which the excitation is small. This behavior may be understood as a consequence of the low-frequency component of the excitation in figure 13; in the limit of a continuous sum over all frequencies, the wave tends towards a delta-comb function with an infinite length between peaks. The incomplete summation in this case may lead to the long, but finite, stretches between wave peaks.

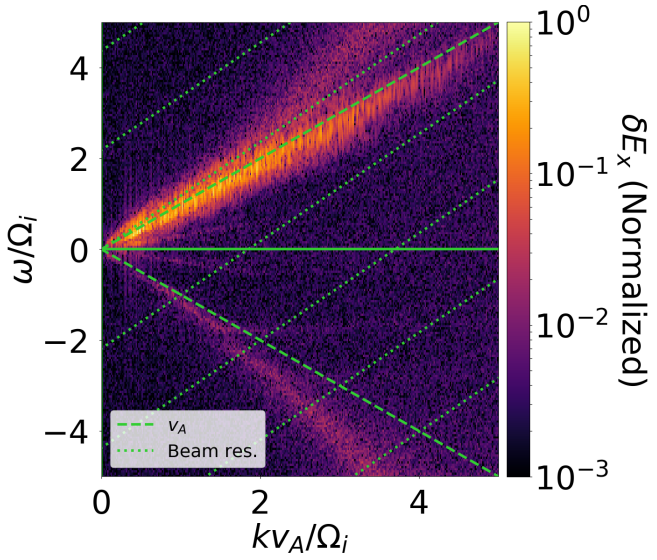

FIG. 13: The dispersion relation for the longitudinal (electrostatic) component for a boron-11 plasma for oblique propagation ($\theta_k = 75°$) with a proton beam population injected at $\theta_b = 60°$.

Regarding enhancement of the fusion rate, some ion acceleration is seen, similar to that seen in section V. In this case, however, the fusion is of the beam-target nature, so any enhancement is more modest compare to the baseline level. It should also be noted that this simulation has been made with parameters mimicking C-2U, while those of future pB^{11} experiments may be somewhat different. Nonetheless, a successor FRC scheme in the model of C-2U would likely feature an ion beta $\beta < 1$ in the SOL. This work seeks only draw attention to a fundamental difference between B^{11} and deuterium as a background plasma species. Additionally, these results suggest that maintaining a relatively low beta of $\beta = 0.1$ in the SOL of these experiments may be beneficial for fusion enhancement, despite any otherwise different parameters.

IX. CONCLUSIONS

This work has surveyed many of the beam-driven modes that can potentially exist in the SOL of an FRC geometry, examining that of the C-2U FRC experiment as an exemplar. For a uniform deuterium plasma and hydrogen (proton) beam, a scan was conducted over the wave propagation and beam injection angles between 0° and 90°. The observation of an enhanced fusion rate in the C-2U experiment provides the chief impetus for this study. In particular, the mode responsible should preferably not cause turbulence or bulk temperature increase, as such effects would be observable through various means such as loss of confinement. The capacity for modes in each angular regime for generating fusion enhancement though ion accelerating has been thus evaluated. As the fundamental linear physics is treated, these results are also potentially applicable to devices of similar parameters, particularly $\beta < 1$ and a large beam pressure.

For instance, such conditions may be found in the magnetopause, the boundary between the terrestrial and stellar magnetic fields, where high-energy particles from the solar wind may act similarly to the beam species examined here[48], or in active galactic nuclei, where the physics examined here has relevance to the wave activity level and evolution of jets, halos, and lobes[49]. The nonlinear physics of ion acceleration and bunching evidenced by ion-Bernstein modes furthermore relies on very similar physics to that seen in ion-driven wakefield acceleration, particularly with regard to the self-modulation instability[45]. Within this experimentally motivated regime, the linear physics of each regime can be briefly summarized.

The regime of parallel propagation ($\theta_k \approx 0°$) predominantly features two circularly polarized shear Alfvén modes, either of which may be excited depending on the beam resonance condition, which in turn depends on the beam injection angle. In both cases, left-handed modes strongly resonate with ions and can lead to a bulk increase in the perpendicular temperature of the ion population. The mode excitation is generally less robust for perpendicular beam injection, but an increased preference for left-handed modes in this case partially compensates for this effect with regard to ion acceleration. In the case of the C-2U experiment, where beam injection is nearly perpendicular to the external magnetic field, it is expected that the latter situation would be more likely. These modes have also been used extensively for ion-cyclotron resonance heating (ICRH), both increasing the plasma temperature and plugging a mirror geometry. Such heating normally incurs the AIC instability (which goes by the same name as the beam-driven mode examined here but is caused by temperature anisotropy), however, which scatters particles into the loss cone. Significant perpendicular heating and loss of confinement in this manner has not been observed on the C-2U experiment. If this mode is present in the SOL in this case, its effects are (thankfully) sufficiently subtle to neglect.

In the regime of oblique propagation, $\theta_k \approx 60°$, the circularly polarized shear Alfvén modes are replaced by linearly polarized compressional and shear Alfvén modes. While the former mode can be prominent even in near-perpendicular propagation, the latter cannot propagate in the limit $\theta_k \to 90°$. Ion acceleration in the oblique propagation regime is generally modest, but is strongest for parallel beam injection. For the C-2U experiment then, and similar devices, it may be possible to neglect the effects of these modes.

The most interesting regime occurs for near-perpendicular propagation, $\theta_k \approx 90°$. Here, electrostatic ion-Bernstein modes rise to prominence at the beam cyclotron harmonics and alter the dispersion of the com-

pressional Alfvén mode. With perpendicular beam injection, the beam resonance lines form Doppler-shifted resonances with the compressional Alfvén mode, which we identify as the magnetoacoustic instability. The exclusively fast phase velocity, electrostatic nature, and discreteness in mode structure for this mode afford efficient acceleration of a fast-ion tail without increasing the ion temperature. This tail in turn dramatically increases the fusion rate by $P/P_{th} > 10^4$ without incurring instabilities from temperature anisotropy.

The fast phase velocity (v_A) of this mode allows a high saturation amplitude, found more familiarly in the field of wakefield acceleration. This saturation level is almost solely dependent on the phase velocity of the wave, departing from the typical physics of quasilinear saturation. Thus the wave can remain robust without strongly affecting the bulk structure of the plasma. Rather, a small population of the fastest ions are accelerated to very high energies while leaving the bulk plasma intact, driving the large increase in fusion rate without creating turbulence. The fusion enhancement from this mode scales according to a power law for a wide range of beam energies.

The electrostatic nature of this mode offers a potential method for targeted excitation. If the density of the beam is bunched at the wavelength of the mode, $\lambda = \pi v_A/\Omega_i$, the mode reaches saturation immediately rather than exponentially growing from noise, and the real-space structure of the wave becomes even more robust and coherent. This purified excitation catalyzes ion acceleration, creating more fusion enhancement than in the case without bunching. With beam velocities beyond $v_b/v_{ti} \approx 16$, however, the benefits to fusion enhancement from bunching appear to diminish, likely because of a change in the fundamental mode structure. The capacity of the plasma to be so particularly excited by this mode also suggests that ICRH tailored to this mode (rather than the AIC mode) may effectively fulfill part of the role of the beam. The mode may then be excited directly, energizing the plasma ions in a targeted manner.

One of the future goals of the successor experiments to C-2U is the achievement of a burning pB^{11} plasma, warranting a brief examination of the analogy of this magnetoacoustic mode in such a plasma. While boron-11 and deuterium have nearly identical cyclotron frequencies, a difference in the species plasma frequencies owing to the +5 charge of boron-11 effectively diminishes the role of the beam, muting the beneficial magnetoacoustic mode seen in the deuterium plasma case. Instead, continuum modes, such as the compressional Alfvén mode, are favored for electrostatic activity. Some ion acceleration is seen, but the contribution of such to the fusion rate is likely small relative to the beam-target contribution. However, this examination was done for C-2U parameters, and the physics is likely somewhat different for a pB^{11}-burning plasma. Future work should more closely at realistic parameters for these plasma species.

While linear plasma wave physics is a well-trod path[32,33], the microscopic beam-driven phenomena of the SOL in an FRC geometry warrant a clear theoretical understanding. In addressing this goal, the accelerator physics at the heart of the C-2U and related experiments perhaps inevitably comes to the fore. These results suggest that the field of accelerator physics may be further harnessed to in the support of fusion efforts.

REFERENCES

[1] L. C. Steinhauer, "Review of field-reversed configurations," Phys. Plasmas **18**, 070501 (2011).

[2] M. W. Binderbauer *et al.*, "A high performance field-reversed configuration," Phys. Plasmas **22**, 056110 (2015).

[3] M. W. Binderbauer *et al.*, "Recent breakthroughs on C-2U: Norman's legacy," AIP Conference Proceedings **1721**, 030003 (2016).

[4] T. Tajima and J. M. Dawson, "Ion cyclotron resonance heating and the Alfvén-ion cyclotron instability," Nucl. Fusion **20**, 1129 (1980).

[5] W. E. Drummond and M. N. Rosenbluth, "Anomalous diffusion arising from microinstabilities in a plasma," Phys. Fluids **5**, 1507 (1962).

[6] D. R. Dakin, T. Tajima, G. Benford, and N. Rynn, "Ion heating by the electrostatic ion cyclotron instability: theory and experiment," J. Plasma Phys. **15**, 175 (1976).

[7] R. Magee, T. Roche, M. Thompson, M. Tobin, M. Beall, B. Deng, and S. Korepanov, "Experimental characterization of Alfvén modes in a field-reversed configuration plasma," Nucl. Fusion **58**, 082011 (2018).

[8] R. Magee, A. Necas, R. Clary, S. Korepanov, S. Nicks, T. Roche, M. Thompson, M. Binderbauer, and T. Tajima, "Direct observation of ion acceleration from a beam-driven wave in a magnetic fusion experiment," Nat. Phys. **15**, 281 (2019).

[9] B. S. Nicks, A. Necas, R. Magee, T. Roche, and T. Tajima, "Wakefield acceleration with ion cyclotron resonance," Phys. Rev. Lett. (Submitted, 2020).

[10] I. B. Bernstein and R. M. Kulsrud, "Ion wave instabilities," Phys. Fluids **3**, 937 (1960).

[11] M. S. Kovner, "Instability of low-frequency electromagnetic waves in a plasma traversed by a beam of charged particles," JETP **40**, 369 (1961).

[12] E. S. Weibel, "Ion cyclotron instability," Phys. Fluids **13**, 3003 (1970).

[13] M. Yamada, S. Seiler, H. W. Hendel, and H. Ikezi, "Electrostatic ion cyclotron instabilities driven by parallel ion beam injection," Phys. Fluids **20**, 450–458 (1977).

[14] E. G. Harris, "Unstable plasma oscillations in a magnetic field," Phys. Rev. Lett. **2**, 34 (1959).

[15] H. Böhmer, "Excitation of ion cyclotron harmonic waves with an ion beam of high perpendicular energy," Phys. Fluids **19**, 1371 (1976).

[16] R. Chang and M. Porkoláb, "Experimental observation of the Harris-type ion beam cyclotron instability," Nucl. Fusion **16**, 142 (1976).

[17] R. O. Dendy, C. N. Lashmore-Davies, and K. F. Kam, "A possible excitation mechanism for observed superthermal ion cyclotron emission from tokamak plasmas," Phys. Fluids B-Plasma **4**, 3996 (1992).

[18] R. O. Dendy, K. G. McClements, C. N. Lashmore-Davies, R. Majeski, and S. Cauffman, "A mechanism for beam-driven excitation of ion cyclotron harmonic waves in the tokamak fusion test reactor," Phys. Plasmas **1**, 3407 (1994).

[19] L. Carbajal, R. O. Dendy, S. C. Chapman, and J. W. S. Cook, "Linear and nonlinear physics of the magnetoacoustic cyclotron instability of fusion-born ions in relation to ion cyclotron emission," Phys. Plasmas **21**, 012106 (2014).

[20] R. O. Dendy and K. G. McClements, "Ion cyclotron emission from fusion-born ions in large tokamak plasmas: a brief review

from JET and TFTR to ITER," Plasma Phys. Contr. F. **57**, 044002 (2015).
[21]W. Heidbrink, E. Fredrickson, T. Mau, C. Petty, R. Pinsker, M. Porkolab, and B. Rice, "High harmonic ion cyclotron heating in DIII-D: Beam ion absorption and sawtooth stabilization," Nucl. Fusion **39**, 1369 (1999).
[22]P. M. Kintner, M. C. Kelley, R. D. Sharp, A. G. Ghielmetti, M. Temerin, C. Cattell, P. F. Mizera, and J. F. Fennell, "Simultaneous observations of energetic (keV) upstreaming and electrostatic hydrogen cyclotron waves," J. Geophys. Res-Space **84**, 7201 (1979).
[23]C. Cattell, "The relationship of field-aligned currents to electrostatic ion cyclotron waves," J. Geophys. Res-Space **86**, 3641 (1981).
[24]H. Okuda and K.-I. Nishikawa, "Ion-beam-driven electrostatic hydrogen cyclotron waves on auroral field lines," J. Geophys. Res-Space **89**, 1023 (1984).
[25]K. I. Golden, L. M. Linson, and S. A. Mani, "Ion streaming instabilities with application to collisionless shock wave structure," Phys. Fluids **16**, 2319 (1973).
[26]F. W. Perkins, "Ion-streaming instabilities: Electromagnetic and electrostatic," Phys. Fluids **19**, 1012 (1976).
[27]S. P. Gary, C. W. Smith, M. A. Lee, M. L. Goldstein, and D. W. Forslund, "Electromagnetic ion beam instabilities," Phys. Fluids **27**, 1852 (1984).
[28]S. P. Gary, C. D. Madland, and B. T. Tsurutani, "Electromagnetic ion beam instabilities: II," Phys. Fluids **28**, 3691 (1985).
[29]S. P. Gary, "Electromagnetic ion/ion instabilities and their consequences in space plasmas: A review," Space Sci. Rev. **56**, 373 (1991).
[30]R. C. Davidson and J. M. Ogden, "Electromagnetic ion cyclotron instability driven by ion energy anisotropy in high-beta plasmas," Phys. Fluids **18**, 1045 (1975).
[31]T. Tajima, K. Mima, and J. M. Dawson, "Alfvén ion-cyclotron instability: Its physical mechanism and observation in computer simulation," Phys. Rev. Lett. **39**, 201 (1977).
[32]T. H. Stix, *The Theory of Plasma Waves* (McGraw-Hill, New York, 1962).
[33]S. Ichimaru, *Basic Principles of Plasma Physics* (W. J. Benjamin, Inc., Reading, MA, 1973).
[34]W. Drummond and D. Pines, "Non-linear stability of plasma oscillations," Nucl. Fus. Suppl. , 1049 (1962).
[35]L. M. Al'Tshul' and V. I. Karpman, "Theory of nonlinear oscillations in a collisionless plasma," JETP **22**, 361 (1966).
[36]T. Tajima and J. M. Dawson, "Laser electron accelerator," Phys. Rev. Lett. **43**, 267 (1979).
[37]T. O'Neil, "Collisionless damping of nonlinear plasma oscillations," Phys. Fluids **8**, 2255 (1965).
[38]B. D. Fried and S. D. Conte, *The Plasma Dispersion Function* (Academic Press, 1961).
[39]S. J. Buchsbaum, "Resonance in a plasma with two ion species," Phys. Fluids **3**, 418 (1960).
[40]D. Welch, D. Rose, B. Oliver, and R. Clark, "Simulation techniques for heavy ion fusion chamber transport," Nucl. Instrum. Meth. A **464**, 134 (2001), pfoc. of the 13th Int. Symp. on Heavy Ion Intertial Fusion.
[41]A. Friedman, "A second-order implicit particle mover with adjustable damping," J. Comput. Phys. **90**, 292 (1990).
[42]R. L. Stenzel, "Whistler waves in space and laboratory plasmas," J. Geophys. Res-Space **104**, 14379 (1999).
[43]E. D. Fredrickson, N. Gorelenkov, C. Z. Cheng, R. Bell, D. Darrow, D. Johnson, S. Kaye, B. LeBlanc, J. Menard, S. Kubota, and W. Peebles, "Observation of compressional Alfvén modes during neutral-beam heating on the national spherical torus experiment," Phys. Rev. Lett. **87**, 145001 (2001).
[44]A. Petrenko, K. Lotov, and A. Sosedkin, "Numerical studies of electron acceleration behind self-modulating proton beam in plasma with a density gradient," Nucl. Instrum. Meth. A **829**, 63 (2016), 2nd European Advanced Accelerator Concepts Workshop - EAAC 2015.
[45]E. Adli *et al.*, "Acceleration of electrons in the plasma wakefield of a proton bunch," Nature (London) **561**, 363 (2018).
[46]K. Mima, J. Fuchs, T. Taguchi, J. Alvarez, J. Marquè, S. Chen, T. Tajima, and J. Perlado, "Self-modulation and anomalous collective scattering of laser produced intense ion beam in plasmas," Matter and Radiation at Extremes **3**, 127 (2018).
[47]A. Caldwell, L. Konstantin, A. Pukhov, and F. Simon, "Proton-driven plasma-wakefield acceleration," Nat. Phys. **5**, 363 (209).
[48]S.-I. Akasofu, *Physics of magnetospheric substorms* (D. Reidel Pub. Co., Dordrecht, Holland, 1977).
[49]A. H. Bridle and R. A. Perley, "Extragalactic radio jets," Annu. Rev. Astron. Astrophys. **22**, 319–358 (1984).